J|A|C|S ARTICLES

Published on Web 07/08/2010

Quantitative 2D and 3D Γ-HCP Experiments for the Determination of the Angles α and ζ in the Phosphodiester Backbone of Oligonucleotides

Senada Nozinovic,[†] Christian Richter,[†] Jörg Rinnenthal,[†] Boris Fürtig,[†,§] Elke Duchardt-Ferner,[‡] Julia E. Weigand,[‡] and Harald Schwalbe*[,†]

Institute for Organic Chemistry and Chemical Biology and Institute for Molecular Biosciences, Center for Biomolecular Magnetic Resonance, Johann Wolfgang Goethe-University Frankfurt, Max-von-Laue-Strasse 7, 60438 Frankfurt am Main, Germany

Received November 26, 2009; E-mail: schwalbe@nmr.uni-frankfurt.de

Abstract: The quantitative Γ-(HCP) experiment, a novel heteronuclear NMR pulse sequence for the determination of the RNA backbone angles $\alpha(O3'_{i-1}-P_i-O5'_i-C5'_i)$ and $\zeta(C3'_i-O3'_i-P_{i+1}-O5'_{i+1})$ in ^{13}C-labeled RNA, is introduced. The experiment relies on the interaction between the CH bond vector dipole and the ^{31}P chemical shift anisotropy (CSA), which affects the relaxation of the $^{13}C,^{31}P$ double- and zero-quantum coherence and thus the intensity of the detectable magnetization. With the new pulse sequence, five different cross-correlated relaxation rates along the phosphodiester backbone can be measured in a quantitative manner, allowing projection-angle and torsion-angle restraints for the two backbone angles α and ζ to be extracted. Two versions of the pulse sequence optimized for the CH and CH_2 groups are introduced and demonstrated for a 14-mer cUUCGg tetraloop RNA model system and for a 27-mer RNA with a previously unknown structure. The restraints were incorporated into the calculation of a very high resolution structure of the RNA model system (Nozinovic, S.; et al. *Nucleic Acids Res.* **2010**, *38*, 683). Comparison with the X-ray structure of the cUUCGg tetraloop confirmed the high quality of the data, suggesting that the method can significantly improve the quality of RNA structure determination.

Introduction

NMR spectroscopy has a major role in RNA structure determination. The availability of isotope-labeled RNAs[1−5] has enabled the development of experiments for the measurement of *J*(X,H) and *J*(H,H) coupling constants,[6] residual dipolar couplings (RDCs),[7] and cross-correlated relaxation rates (Γ).[8,9] The determination of a large number of independent NMR restraints is a prerequisite for obtaining high-resolution RNA structures by NMR spectroscopy. In comparison with proteins, RNA oligonucleotides possess a larger number of degrees of freedom in the phosphodiester backbone, and determination of the conformation (especially of the backbone) is difficult because of the low proton density. In proteins, the backbone conformation is described by the Ramachandran diagram, which shows the correlation of ϕ and ψ in torsion-angle space. In RNA, the corresponding ζ_i,α_{i+1} correlation diagram (Figure 1A,B) defines the two torsions around the phosphorus atom along the 5′,3′ chain direction of RNA.[10] Therefore, determination of experimental restraints for the two backbone torsions ζ and α is of considerable importance in any conformational analysis of RNA structure. At the same time, the angles $\alpha(O3'_{i-1}-P_i-O5'_i-C5'_i)$ and $\zeta(C3'_i-O3'_i-P_{i+1}-O5'_{i+1})$ are particularly difficult to determine by NMR spectroscopy because the phosphorus atom is bound only to non-NMR-active oxygen atoms. Qualitative estimates of these two angles are usually derived from analysis of ^{31}P chemical shifts, but such an analysis can be used only to exclude the trans conformation.[11,12] Another NMR parameter that reflects the conformation of the RNA backbone with regard to the torsion angles α and ζ is the residual chemical shift anisotropy (rCSA) obtained for aligned RNA samples.[13] However, both of these parameters, the ^{31}P chemical shift and the

[†] Institute for Organic Chemistry and Chemical Biology, Johann Wolfgang Goethe-University Frankfurt.
[‡] Institute for Molecular Biosciences, Johann Wolfgang Goethe-University Frankfurt.
[§] Present address: Department of Biochemistry, Max F. Perutz Laboratories, 1030 Vienna, Austria.

(1) Batey, R. T.; Inada, M.; Kujawinski, E.; Puglisi, J. D.; Williamson, J. R. *Nucleic Acids Res.* **1992**, *20*, 4515.
(2) Batey, R. T.; Battiste, J. L.; Williamson, J. R. *Methods Enzymol.* **1995**, *261*, 300.
(3) Nikonowicz, E. P.; Sirr, A.; Legault, P.; Jucker, F. M.; Baer, L. M.; Pardi, A. *Nucleic Acids Res.* **1992**, *20*, 4507.
(4) Quant, S.; Wechselberger, R. W.; Wolter, M. A.; Wörner, K. H.; Schell, P.; Engels, J. W.; Griesinger, C.; Schwalbe, H. *Tetrahedron Lett.* **1994**, *35*, 6649.
(5) Lagoja, I. M.; Herdewijn, P. *Synthesis* **2002**, 301.
(6) Marino, J. P.; Schwalbe, H.; Griesinger, C. *Acc. Chem. Res.* **1999**, *32*, 614.
(7) Boisbouvier, J.; Delaglio, F.; Bax, A. *Proc. Natl. Acad. Sci. U.S.A.* **2003**, *100*, 11333.
(8) Reif, B.; Hennig, M.; Griesinger, C. *Science* **1997**, *276*, 1230.
(9) Reif, B.; Diener, A.; Hennig, M.; Maurer, M.; Griesinger, C. *J. Magn. Reson.* **2000**, *143*, 45.
(10) Schneider, B.; Moravek, Z.; Berman, H. M. *Nucleic Acids Res.* **2004**, *32*, 1666.
(11) Gorenstein, D. G. *Phosphorus-31 NMR: Principles and Applications*; Academic Press: New York, 1984.
(12) Varani, G.; Aboul-ela, F.; Allain, F. H. T. *Prog. Nucl. Magn. Reson. Spectrosc.* **1996**, *29*, 51.
(13) Wu, Z.; Tjandra, N.; Bax, A. *J. Am. Chem. Soc.* **2001**, *123*, 3617.

10.1021/ja910015n

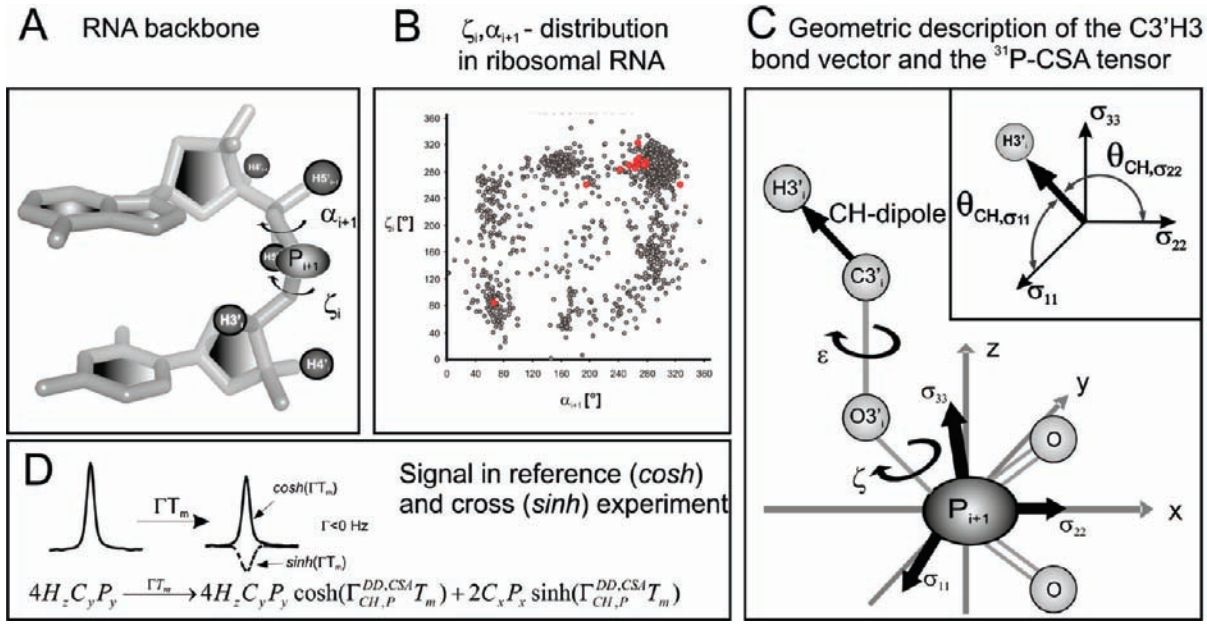

Figure 1. (A) RNA backbone with notation of the torsion angles ζ_i and α_{i+1} and the backbone CH bond vectors (C3′H3′, C4′H4′, and C5′H5′/H5″) that interact with the ^{31}P CSA. (B) ζ_i,α_{i+1} distributions found in (gray) ribosomal RNA (PDB entry 1ffk)[23] and (red) the 14-mer cUUCGg tetraloop RNA (PDB entry 2koc).[24] (C) Orientation of the C3′H3′ bond vector and the ^{31}P CSA tensor (σ_{11}, σ_{22}, σ_{33}) with respect to the molecular coordinate frame (*x*, *y*, *z*) as defined elsewhere.[25] (D) Pictorial illustration of a signal before and after the mixing time, with the proportion of the intensities adjusted for clarity. According to eq 2, DQC/ZQC of the type $4H_zC_yP_y$ evolves under cross-correlated relaxation and splits into cosh- and sinh-modulated components that are selected separately in the reference and cross experiments, respectively.

residual chemical shift anisotropy, are indirect, often only semiquantitative, and difficult to measure because of low ^{31}P spectral resolution. In fact, in NMR structure determinations, the two torsion angles are often set to canonical values.

In 2000, Richter et al.[14] proposed an experiment to determine the RNA backbone angles α and ζ. The experiment relied on the quantification of CH dipolar and ^{31}P CSA cross-correlated relaxation that evolves in spectra of ^{13}C,^{31}P double- and zero-quantum coherence (DQC/ZQC). In the original experiment, ^{13}C,^{31}P DQC/ZQC was allowed to evolve under the influence of scalar *J*(C,H) coupling and cross-correlated relaxation for a constant time period. The observed signal in the evolution period was a multiplet split by *J*(C,H) scalar couplings. By quantification of the differences in the intensities of the multiplet components, the desired rate $\Gamma_{CH,P}^{DD,CSA}$ could be extracted.

Here we propose a fundamentally different and improved method that is more sensitive and provides higher resolution. The novel pulse sequences allow the measurement of five different cross-correlated relaxation rates in a quantitative correlation experiment.[15−18] We demonstrate the measurement and quantitative analysis of the Γ rates for the 14-mer cUUCGg tetraloop RNA model system and discuss the practical aspects of the incorporation of cross-correlated relaxation rates $\Gamma_{CH,P}^{DD,CSA}$ into an RNA structure calculation protocol as torsion-angle restraints. We show that this precious information about the backbone angles α and ζ can be obtained especially for noncanonical regions in the RNA structure, where chemical-shift-based restraining of torsion angles to the standard A-form geometry is not possible. We also apply the new pulse sequence to a 27-mer neomycin riboswitch RNA with an unknown structure.[19,20] Finally, we discuss a qualitative analysis of the Γ rates in the context of 32 different conformational classes of RNA that reveals the capacity of the new method to discriminate between the possible RNA backbone conformations.

Materials and Methods

A 14-mer cUUCGg tetraloop RNA sample with the sequence 5′-PO_4^{2-}-PO_3^--PO_3^--GGCAC(UUCG)GUGCC-3′ was purchased from Silantes GmbH (Munich, Germany). Samples for NMR spectroscopy contained ∼0.7 mM RNA in 20 mM potassium phosphate (pH 6.4), 0.4 mM EDTA, and 100% D_2O. ^{1}H chemical shifts were referenced directly to trimethylsilyl propionate (TSP) as an external reference. NMR chemical shift assignments for ^{1}H, ^{13}C, ^{15}N, and ^{31}P resonances have been published.[21] NMR experiments were carried out at 298 K on a Bruker AV 600 MHz spectrometer equipped with a 5 mm *z*-axis gradient ^{1}H(^{13}C,^{31}P)-TCI cryogenic probe. The data were processed and analyzed using the program TOPSPIN 2.1 (Bruker Biospin).

A uniformly ^{13}C/^{15}N-labeled 27-mer RNA with sequence 5′-PO_4^{2-}-PO_3^--PO_3^--GGCUGCUUGUCCUUUAAUGGUCCAGUC-cyclicPO_2^--3′ was synthesized by in vitro transcription with T7 RNA polymerase using commercially available isotope-labeled nucleotide triphosphates (Silantes GmbH) and linearized plasmid DNA as a template. The primary RNA transcripts contained a hammerhead ribozyme in cis in order to generate uniform 3′ ends. Processed transcripts corresponding to the correctly cleaved 27-mer were purified by preparative denaturing polyacrylamide gel

(14) Richter, C.; Reif, B.; Griesinger, C.; Schwalbe, H. *J. Am. Chem. Soc.* **2000**, *122*, 12728.
(15) Pelupessy, P.; Chiarparin, E.; Ghose, R.; Bodenhausen, G. *J. Biomol. NMR* **1999**, *13*, 375.
(16) Felli, I. C.; Richter, C.; Griesinger, C.; Schwalbe, H. *J. Am. Chem. Soc.* **1999**, *121*, 1956.
(17) Duchardt, E.; Richter, C.; Ohlenschläger, O.; Görlach, M.; Wöhnert, J.; Schwalbe, H. *J. Am. Chem. Soc.* **2004**, *126*, 1962.
(18) Rinnenthal, J.; Richter, C.; Ferner, J.; Duchardt, E.; Schwalbe, H. *J. Biomol. NMR* **2007**, *39*, 17.
(19) Weigand, J. E.; Sanchez, M.; Gunnesch, E.-B.; Zeiher, S.; Schroeder, R.; Suess, B. *RNA* **2008**, *14*, 89.
(20) Duchardt-Ferner, E.; Weigand, J. E.; Ohlenschläger, O.; Schmidtke, S. R.; Süss, B.; Wöhnert, J. *Angew. Chem., Int. Ed.*, accepted.
(21) Fürtig, B.; Richter, C.; Bermel, W.; Schwalbe, H. *J. Biomol. NMR* **2004**, *28*, 69.

electrophoresis following standard protocols. The aminoglycoside ribostamycin was added to the purified RNA at a ratio of 1:1. The sample concentration of the ribostamycin−RNA complex was 1.1 mM in NMR buffer containing 25 mM potassium phosphate (pH 6.2) and 50 mM KCl in 100% (v/v) D_2O. The NMR chemical shift assignment has been published.[22]

Theoretical Basis

In addition to the overall correlation time τ_c, cross-correlated relaxation between the CH dipole and the ^{31}P CSA depends on the projection angles $\theta_{CH,\sigma_{nn}}$ between the CH bond vector and the ^{31}P CSA tensor components (σ_{11}, σ_{22}, σ_{33}) (Figure 1C). The projection angles are functions of the interconnecting backbone torsion angles [e.g., ε and ζ for the C3′H3′ dipole (see Figure 1C)], and therefore, the torsion angles can be determined from cross-correlated relaxation rates.

The cross-correlated relaxation rate is given by:

$$\Gamma_{CH,P}^{DD,CSA} = -\frac{2}{15}\gamma_P B_0 \tau_c \hbar \frac{\mu_0}{4\pi}\frac{\gamma_H \gamma_C}{r_{CH}^3}\left[(\sigma_{11}-\sigma_{33})(3\cos^2\theta_{CH,\sigma_{11}}-1)+(\sigma_{22}-\sigma_{33})(3\cos^2\theta_{CH,\sigma_{22}}-1)\right] \quad (1)$$

in which the σ_{nn} are the diagonal elements of the ^{31}P CSA tensor ($\sigma_{11} = -86$ ppm, $\sigma_{22} = -26$ ppm, $\sigma_{33} = 112$ ppm)[26] (for discussion, see below), γ_N is the gyromagnetic ratio of nucleus N, B_0 is the field strength, r_{CH} is the the CH bond length, $\hbar$ is Planck's constant divided by 2π, and μ_0 is the magnetic susceptibility of vacuum. The overall rotational correlation time τ_c for the 14-mer RNA is 2.27 ns at 298 K.[27]

The novel quantitative Γ-HCP experiment is derived from the HCP experiment[28] and requires a ^{13}C-labeled sample. The coherence transfer pathway is different in experiments optimized for the CH (C2′H2′, C3′H3′, C4′H4′) and CH_2 [C5′H5′(pro-*R*)/H5″(pro-*S*)] groups, as will be discussed below.

CH Groups. $\Gamma^{DD,CSA}_{(C2'H2')_i,P_{i+1}}$, $\Gamma^{DD,CSA}_{(C3'H3')_i,P_{i+1}}$, $\Gamma^{DD,CSA}_{(C4'_iH4'_i),P_i}$ and $\Gamma^{DD,CSA}_{(C4'_iH4'_i),P_{i+1}}$ cross-correlated relaxation rates can be measured in 2D and 3D experiments based on the same coherence transfer pathway. In two consecutive INEPT steps followed by a *z* filter element (sections a−c in Figure 2A), DQC/ZQC of the type $4H_zC_yP_y$ is created at section c in the pulse sequence (Figure 2A). Through cross-correlated relaxation, this initially generated DQC/ZQC $4H_zC_yP_y$ evolves into two terms during the mixing time T_m according to[16,29]

$$4H_zC_yP_y \xrightarrow{\hat{\Gamma}[P_{z'}[2C_zH_z]]} 4H_zC_yP_y\cosh(\Gamma_{CH,P}^{DD,CSA}T_m) + 2C_xP_x\sinh(\Gamma_{CH,P}^{DD,CSA}T_m) \quad (2)$$

The Γ rate is extracted from the intensity ratio of the cosh- and sinh-modulated signals (Figure 1D), yielding a tanh-dependent modulation of the rate:

$$\tanh(\Gamma T_m) = \frac{\sinh(\Gamma T_m)}{\cosh(\Gamma T_m)} = \frac{I_{cross}}{I_{ref}} \quad (3)$$

where I_{cross} and I_{ref} represent the signals in the cross and reference experiments, respectively.

Therefore, two experiments, a reference experiment and a cross experiment, must be recorded to select either one of the two operators. After the mixing time T_m (section c in Figure 2A) in the reference experiment, through application of a second *z* filter, gradients, and phase cycling, only the cosh-modulated term is detected. Additionally, a ^{31}P chemical shift evolution period (section d in Figure 2A) can be introduced in order to differentiate between the $\Gamma^{DD,CSA}_{(C4'_iH4'_i),P_i}$ and $\Gamma^{DD,CSA}_{(C4'_iH4'_i),P_{i+1}}$ cross-correlated relaxation rates. Such differentiation was not possible in the previously published pulse sequence. ^{13}C chemical evolution occurs in a constant-time manner during the second, refocusing ^{13}C,^{31}P-INEPT step (section e in Figure 2A). Finally, the double-antiphase coherence $4H_zC_yP_y$ is then converted into detectable ^{1}H single-quantum coherence in two INEPT steps in a sensitivity-enhanced manner.[30−32]

In the cross experiment, the second *z* filter with a phase shift (section e in Figure 2A) allows the sinh-modulated term $[2C_xP_x\sinh(\Gamma^{DD,CSA}_{CH,P}T_m)]$ to pass. After ^{13}C and optional ^{31}P chemical shift evolution, an additional delay $\{\Delta'' = 1/[2^1J(C,H)]\}$ is introduced (section e in Figure 2A) for proton−carbon recoupling to convert CH in-phase coherence into CH antiphase coherence, which finally can be transferred to a detectable ^{1}H signal as in the reference experiment. The cross-correlated relaxation rate can be extracted according to eq 4:

$$\Gamma_{CH,P}^{DD,CSA} = \frac{1}{T_m}\tanh^{-1}\left(\frac{I_{cross}}{I_{ref}}\right)\frac{NS_{ref}}{NS_{cross}} \quad (4)$$

where NS_{cross} and NS_{ref} are the numbers of scans in the cross and reference experiments, respectively.

In summary, the above-described pulse sequence optimized for the CH group can be implemented in three versions to measure $\Gamma^{DD,CSA}_{(C2'H2')_i,P_{i+1}}$, $\Gamma^{DD,CSA}_{(C3'H3')_i,P_{i+1}}$, $\Gamma^{DD,CSA}_{(C4'_iH4'_i),P_i}$ and $\Gamma^{DD,CSA}_{(C4'_iH4'_i),P_{i+1}}$ cross-correlated relaxation rates. For $\Gamma^{DD,CSA}_{(C2'H2')_i,P_{i+1}}$ and $\Gamma^{DD,CSA}_{(C3'H3')_i,P_{i+1}}$, it is sufficient to perform a ^{1}H,^{13}C 2D Γ-HC(P) experiment, while $\Gamma^{DD,CSA}_{(C4'_iH4'_i),P_i}$ and $\Gamma^{DD,CSA}_{(C4'_iH4'_i),P_{i+1}}$ can be obtained from either an ^{1}H,^{31}P 2D Γ-H(C)P or ^{1}H,^{13}C,^{31}P 3D Γ-HCP experiment, depending on the resolution of resonances.

CH_2 Groups. For the magnetization transfer and selection of cross-correlated relaxation rates involving a CH_2 group, such as the C5′H5′/H5″ group in RNA/DNA, a different approach is necessary in order to distinguish between the contributions of the two protons [here further termed H^1 for H5′(pro-*R*) and H^2 for H5″(pro-*S*)], which appear at the same carbon frequency in the carbon evolution period t_2. Therefore, a 3D correlation with an ^{1}H chemical shift evolution period is introduced. Furthermore, the magnetization selection is optimized to select only the carbon in-phase operator during the mixing time in both experiments. The pulse sequence starts with the INEPT step, which contains a ^{1}H chemical shift evolution period to distinguish the two methylene protons on the basis of their proton chemical shifts. After the *z* filter, DQC/ZQC is selected. In the cross experiment, the pulse sequence continues with the CH antiphase operator, which undergoes cross-correlated relaxation according to eq 5:[16,29]

(22) Schmidtke, S. R.; Duchardt-Ferner, E.; Weigand, J. E.; Suess, B.; Wöhnert, J. *Biomol. NMR Assignments* **2010**, *4*, 115.
(23) Ban, N.; Nissen, P.; Hansen, J.; Moore, P. B.; Steitz, T. A. *Science* **2000**, *289*, 905.
(24) Nozinovic, S.; Fürtig, B.; Jonker, H. R. A.; Richter, C.; Schwalbe, H. *Nucleic Acids Res.* **2010**, *38*, 683.
(25) Herzfeld, J.; Griffin, R. G.; Haberkorn, R. A. *Biochemistry* **1978**, *17*, 2711.
(26) Přecechtělová, J.; Padrta, P.; Munzarova, M. L.; Sklenář, V. *J. Phys. Chem. B* **2008**, *112*, 3470.
(27) Ferner, J.; Villa, A.; Duchardt, E.; Widjajakusuma, E.; Wöhnert, J.; Stock, G.; Schwalbe, H. *Nucleic Acids Res.* **2008**, *36*, 1928.
(28) Marino, J. P.; Schwalbe, H.; Anklin, C.; Bermel, W.; Crothers, D. M.; Griesinger, C. *J. Am. Chem. Soc.* **1994**, *116*, 6472.
(29) Schwalbe, H.; Carlomagno, T.; Hennig, M.; Junker, J.; Reif, B.; Richter, C.; Griesinger, C. *Methods Enzymol.* **2001**, *338*, 35.
(30) Palmer, A. G.; Cavanagh, J.; Wright, P. E.; Rance, M. *J. Magn. Reson.* **1991**, *93*, 151.
(31) Kay, L. E.; Keifer, P.; Saarinen, T. *J. Am. Chem. Soc.* **1992**, *114*, 10663.
(32) Schleucher, J.; Schwendinger, M.; Sattler, M.; Schmidt, P.; Schedletzky, O.; Glaser, S. J.; Sørensen, O. W.; Griesinger, C. *J. Biomol. NMR* **1994**, *4*, 301.
(33) Roehrl, M. H.; Heffron, G. J.; Wagner, G. *J. Magn. Reson.* **2005**, *174*, 325.
(34) Shaka, A. J.; Barker, P. B.; Freeman, R. J. *J. Magn. Reson.* **1985**, *64*, 547.
(35) Emsley, L.; Bodenhausen, G. *J. Magn. Reson.* **1992**, *97*, 135.

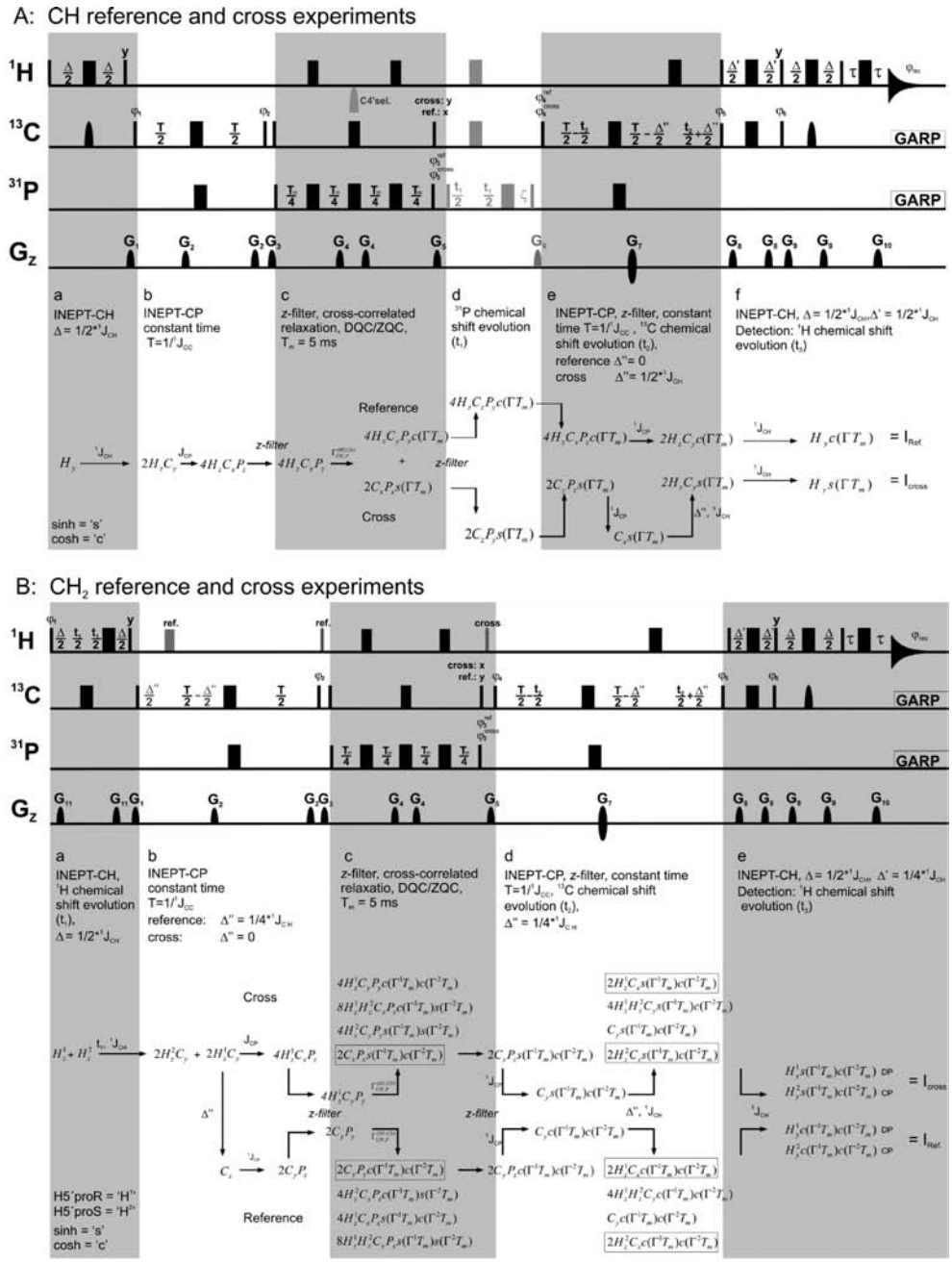

Figure 2. Pulse sequence of the quantitative 2D Γ-HCP and 3D Γ-HCP experiments optimized for (A) CH and (B) CH_2 and summaries of the magnetization transfer pathway in a condensed form as operator formalism (a−f in A and a−e in B). The cosh function is abbreviated as "c" and sinh as "s". Narrow and wide filled bars correspond to rectangular 90 and 180° pulses, respectively. Selective pulses and gradients are indicated as semiellipses. The default pulse phase is *x*. The pulse sequences were optimized on a Bruker spectrometer with the typical Bruker phase settings.[33] The reference and cross experiments are summarized in one-pulse sequence schemes. The proton carrier frequency is centered at the water frequency (4.7 ppm). The values of the ^{13}C and ^{31}P offsets are set to 77 and −1.5 ppm, respectively. T_m is the variable relaxation period. The black semiellipse in the proton−carbon INEPT transfer is a 500 μs smoothed chirp amplitude adiabatic pulse (Bruker Topspin 2.0, 2006) with a 60 kHz sweep and a length of 500 μs. Asynchronous GARP decoupling[34] is used to suppress heteronuclear scalar couplings during acquisition. The pulse field gradients of 1 ms length have a smoothed square amplitude (Bruker Topspin 2.0, 2006). They are applied along the *z* axis and have the following strengths: G_1, −40%; G_2, 25%; G_3, −50%; G_4, −5%; G_5, −45%; G_6, 2%; G_7,80%; G_8, 11%; G_9, −5%; G_{10}, 20.1%; G_{11}, 8%. A gradient strength of 100% corresponds to 53.5 G/cm. (A) The fixed delays are adjusted as follows: $\Delta = 3$ ms $[1/(2^1J_{HC})]$, $\Delta' = 3$ ms $[1/(2^1J_{HC})]$, $T = 25$ ms $[1/(2^1J_{CC})]$, $\tau = 1$ ms (length of G_{10}). In the reference experiment, Δ'' is set to 0 ms, and in the cross experiment, Δ'' is set to 3 ms. In the mixing period, a nonselective 180° pulse is applied on the carbon channel. For each t_2 increment, echo and antiecho coherence transfer pathways are alternately selected by inversion of the polarity of G_7 along with the pulse phase φ_6, and the spectra are processed using the enhanced sensitivity method.[30−32] Axial peaks in the ^{13}C dimension are shifted to the edge of the spectrum by incrementing φ_4 and the receiver phase by 180° for each successive value of t_2. All of the pulses, delays, and gradients for the C4′-selective 3D experiment are shown in gray. For the 3D experiment, a C4′-band-selective 180° pulse Q3 Gaussian cascade[35] of 1.5 ms (gray semiellipse) is applied in the middle of the mixing time, and $\Delta' = 3$ ms. Phase cycling: $\varphi_1 = 8(x), 8(-x)$; $\varphi_2 = 16(y), 16(-y)$; $\varphi_3^{ref} = (x), (-x)$; $\varphi_3^{cross} = (y), (-y)$; $\varphi_4^{ref} = 4(y), 4(-y)$; $\varphi_4^{cross} = 4(x), 4(-x)$; $\varphi_5 = (2x), 2(-x)$; $\varphi_6 = 2(-y), 2(y)$; $\varphi_{rec} = R, -R, -R, R$, where $R = x, 2(-x), x, -x, 2(x), -x$. G_7 and φ_6 are modulated according to echo/antiecho modulation in the ω_2 dimension using sensitivity enhancement.[30−32] (B) The fixed delays are adjusted as follows: $\Delta = 3$ ms $[1/(2^1J_{HC})]$, $\Delta' = 1.5$ ms $[1/(4^1J_{HC})]$, $\Delta'' = 1.5$ ms $[1/(4^1J_{CH})]$, $T = 25$ ms $[1/(2^1J_{CC})]$, $\tau = G_{10}$. Selected operators are highlighted with a box. Phase cycling: $\varphi_1 = 8(x), 8(-x)$; $\varphi_2 = 16(x), 16(-x)$; $\varphi_3^{ref} = (x), (-x)$; $\varphi_3^{cross} = (y), (-y)$; $\varphi_4 = 4(x), 4(-x)$; $\varphi_5 = (2x), 2(-x)$; $\varphi_6 = 2(-y), 2(y)$; $\varphi_{rec} = R, -R, -R, R$, where $R = x, 2(-x), x, -x, 2(x), -x$. G_7 and φ_6 are modulated according to echo/antiecho modulation in the ω_2 dimension using sensitivity enhancement.[30−32]

$$4H_z^1C_yP_y \xrightarrow{\hat{\tilde{\Gamma}}[P_z,[2C_zH_z^1]],\,\hat{\tilde{\Gamma}}[P_z,[2C_zH_z^2]]}$$

$$\begin{aligned} &4H_z^1C_yP_y\cosh(\Gamma_{CH^1,P}^{DD,CSA}T_m)\cosh(\Gamma_{CH^2,P}^{DD,CSA}T_m) + \\ &8H_z^1H_z^2C_xP_x\cosh(\Gamma_{CH^1,P}^{DD,CSA}T_m)\sinh(\Gamma_{CH^2,P}^{DD,CSA}T_m) + \\ &2C_xP_x\sinh(\Gamma_{CH^1,P}^{DD,CSA}T_m)\cosh(\Gamma_{CH^2,P}^{DD,CSA}T_m) + \\ &4H_z^2C_yP_y\sinh(\Gamma_{CH^1,P}^{DD,CSA}T_m)\sinh(\Gamma_{CH^2,P}^{DD,CSA}T_m) \end{aligned} \quad (5)$$

After the mixing time, only the operator

$$2C_xP_x\sinh(\Gamma_{CH^1,P}^{DD,CSA}T_m)\cosh(\Gamma_{CH^2,P}^{DD,CSA}T_m)$$

(i.e., the third term in eq 5) is selected after the two INEPT steps.

In the reference experiment, the first INEPT step is followed by an additional delay $\{\Delta'' = 1/[4^1J(C,H)]\}$ that refocuses the CH antiphase coherence to carbon in-phase coherence, which is then converted into a coherence of the type $2C_yP_y$ (section b in Figure 2B). Such a CH in-phase coherence is needed in order to avoid mixing of the two proton relaxation rates at the same time, and it evolves during the mixing time according to eq 6:

$$2C_yP_y \xrightarrow{\hat{\tilde{\Gamma}}[P_z,[2C_zH_z^1]],\,\hat{\tilde{\Gamma}}[P_z,[2C_zH_z^2]]}$$

$$\begin{aligned} &2C_yP_y\cosh(\Gamma_{CH^1,P}^{DD,CSA}T_m)\cosh(\Gamma_{CH^2,P}^{DD,CSA}T_m) + \\ &4H_z^2C_xP_x\cosh(\Gamma_{CH^1,P}^{DD,CSA}T_m)\sinh(\Gamma_{CH^2,P}^{DD,CSA}T_m) + \\ &4H_z^1C_xP_x\sinh(\Gamma_{CH^1,P}^{DD,CSA}T_m)\cosh(\Gamma_{CH^2,P}^{DD,CSA}T_m) + \\ &8H_z^1H_z^2C_yP_y\sinh(\Gamma_{CH^1,P}^{DD,CSA}T_m)\sinh(\Gamma_{CH^2,P}^{DD,CSA}T_m) \end{aligned} \quad (6)$$

After the mixing time, only the operator

$$2C_yP_y\cosh(\Gamma_{CH^1,P}^{DD,CSA}T_m)\cosh(\Gamma_{CH^2,P}^{DD,CSA}T_m)$$

(i.e., the first term in eq 6) is retained. The contribution of the second proton $[\cosh(\Gamma_{CH^2,P}^{DD,CSA}T_m)]$, which is cosh-modulated in both experiments, can be neglected because it cancels out when the ratio of the signal intensities from the cross and reference experiments is formed.

In both experiments, the in-phase operators must be proton-recoupled before the final INEPT step is introduced. During this time $\{\Delta'' = 1/[4^1J(C,H)]$; section d in Figure 2B$\}$, the magnetization is coupled to both methylene protons, which causes two signals to arise in both dimensions (ω_1, ω_3), either at the frequency of the same proton (the diagonal peak) or that of both protons (the cross-peak). For analysis, the intensity of the reference experiment must be corrected by a factor of 2 because of the additional delay (Δ'') after the first INEPT step. The cross-correlated relaxation rate can be extracted according to eq 4. In both experiments, application of π pulses during the mixing-time period suppresses additional cross-correlated relaxation pathways, including $\Gamma_{PH,P}^{DD,CSA}$, $\Gamma_{CH,C}^{DD,CSA}$, and $\Gamma_{CH,PH}^{DD,DD}$.[16−18]

Results

The new pulse sequence was first applied to a 14-mer cUUCGg tetraloop RNA (Figure 3A). The structure of the cUUCGg tetraloop has been studied extensively using both NMR spectroscopy[18,21,24,27,36−38] and X-ray crystallography[39−41] and therefore serves ideally as a reference. In addition, ^{13}C relaxation studies have been performed previously, so the correlation time for the overall tumbling of the RNA is well-known.[27] Furthermore, the torsion angles β and ε needed for conformational analysis of the Γ rates have been obtained from $^3J(H,P)$ and $^3J(C,P)$ coupling constants.[42] Figure 3 shows the well-resolved quantitative 2D Γ-HC(P) experiment and the $^1H,^{31}P$ plane of the quantitative 3D Γ-H(C)P experiment recorded on the 14-mer cUUCGg tetraloop RNA. As shown in the 1D traces, the cross-peaks in the cross experiment exhibit high signal-to-noise ratios, allowing the cross-correlated relaxation rates to be extracted reliably by integration of the respective cross-peaks. In fact, the resulting cross-correlated relaxation rates for the C5′H5′ groups in the ^{13}C-resolved-only 2D Γ-HC(P) experiment (Figure 3A) represent the sum of the two involved cross-correlated relaxation rates $\Gamma_{(C5'_iH5'_i\text{pro-}R),P_i}^{DD,CSA}$ and $\Gamma_{(C5'_iH5''_i\text{pro-}S),P_i}^{DD,CSA}$ for the two methylene protons. The same is the case for $\Gamma_{(C4'_iH4'_i),P_i}^{DD,CSA}$ and $\Gamma_{(C4'_iH4'_i),P_{i+1}}^{DD,CSA}$ for the C4′H4′ group, where analysis yields the sum of the two cross-correlated relaxation rates because the resonances of the two phosphorus nuclei are not resolved in such a 2D Γ-HC(P) experiment without additional phosphorus chemical shift evolution. However, they contain conformational information, as will be discussed later. Signals of the C4′H4′ groups yielding $\Gamma_{(C4'_iH4'_i),P_i}^{DD,CSA}$ and $\Gamma_{(C4'_iH4'_i),P_{i+1}}^{DD,CSA}$ are well-defined in the ^{31}P-resolved 2D Γ-H(C)P experiment (Figure 3B), with only four overlapping signals that could be resolved in the 3D Γ-HCP experiment involving ^{13}C chemical shift evolution.

Table 1 summarizes the cross-correlated relaxation rates of the 14-mer cUUCGg tetraloop RNA obtained from the 2D and 3D experiments. In total, 52 cross-correlated relaxation rates out of 65 possible ones could be extracted. For each of the stem residues, every cross-correlated relaxation rate except $\Gamma_{(C5'_iH5''_i\text{pro-}S),P_i}^{DD,CSA}$ exhibited a negative value, as predicted for the A-form RNA conformation.

Quantitative analysis of the cross-correlated relaxation rates was performed with the program *Mathematica*.[43] The cross-correlated relaxation rate $\Gamma_{CH,P}^{DD,CSA}$ depends on the projection angle of the CH dipole vector onto the components of the ^{31}P CSA tensor (eq 1, Figure 1C). In order to extract the structural restraints, the dependence of $\Gamma_{CH,P}^{DD,CSA}$ on the projection of each axis of the ^{31}P CSA tensor needs to be known. Originally,[14] information about the ^{31}P CSA was taken from single-crystal NMR data on barium diethylphosphate.[25] Here we utilized the size and orientation of the ^{31}P CSA taken from the recently published density functional theory (DFT) study of the ^{31}P CSA in RNA.[26] On the basis of a recent experimental solid-state NMR investigation, we were able to infer that the CSA magnitude obtained by DFT calculations is valid.[38] Therefore, we implemented the conformational dependence of the CSA as calculated using DFT. The projection angles $\theta_{CH,\sigma}$ depend on the conformation of the phosphodiester backbone. The rates $\Gamma_{(C5'_iH5''_i\text{pro-}S),P_i}^{DD,CSA}$ and $\Gamma_{(C5'_iH5'_i\text{pro-}R),P_i}^{DD,CSA}$, for example, depend on α and β, while the

(36) Duchardt, E.; Schwalbe, H. *J. Biomol. NMR* **2005**, *32*, 295.
(37) Fürtig, B.; Richter, C.; Wöhnert, J.; Schwalbe, H. *ChemBioChem* **2003**, *4*, 936.
(38) Rinnenthal, J.; Richter, C.; Nozinovic, S.; Fürtig, B.; Lopez, J.; Glaubitz, C.; Schwalbe, H. *J. Biomol. NMR* **2009**, *45*, 143.
(39) Ennifar, E.; Nikulin, A.; Tishchenko, S.; Serganov, A.; Nevskaya, N.; Garber, M.; Ehresmann, B.; Ehresmann, C.; Nikonov, S.; Dumas, P. *J. Mol. Biol.* **2000**, *304*, 35.
(40) Tishchenko, S.; Nikulin, A.; Fomenkova, N.; Nevskaya, N.; Nikonov, O.; Dumas, P.; Moine, H.; Ehresmann, B.; Ehresmann, C.; Piendl, W.; Lamzin, V.; Garber, M.; Nikonov, S. *J. Mol. Biol.* **2001**, *311*, 311.
(41) Carter, A. P.; Clemons, W. M.; Brodersen, D. E.; Morgan-Warren, R. J.; Wimberly, B. T.; Ramakrishnan, V. *Nature* **2000**, *407*, 340.
(42) Richter, C.; Reif, B.; Wörner, K.; Quant, S.; Marino, J. P.; Engels, J. W.; Griesinger, C.; Schwalbe, H. *J. Biomol. NMR* **1998**, *12*, 223.
(43) *Mathematica*, version 6.0; Wolfram Research: Champaign, IL, 2007.

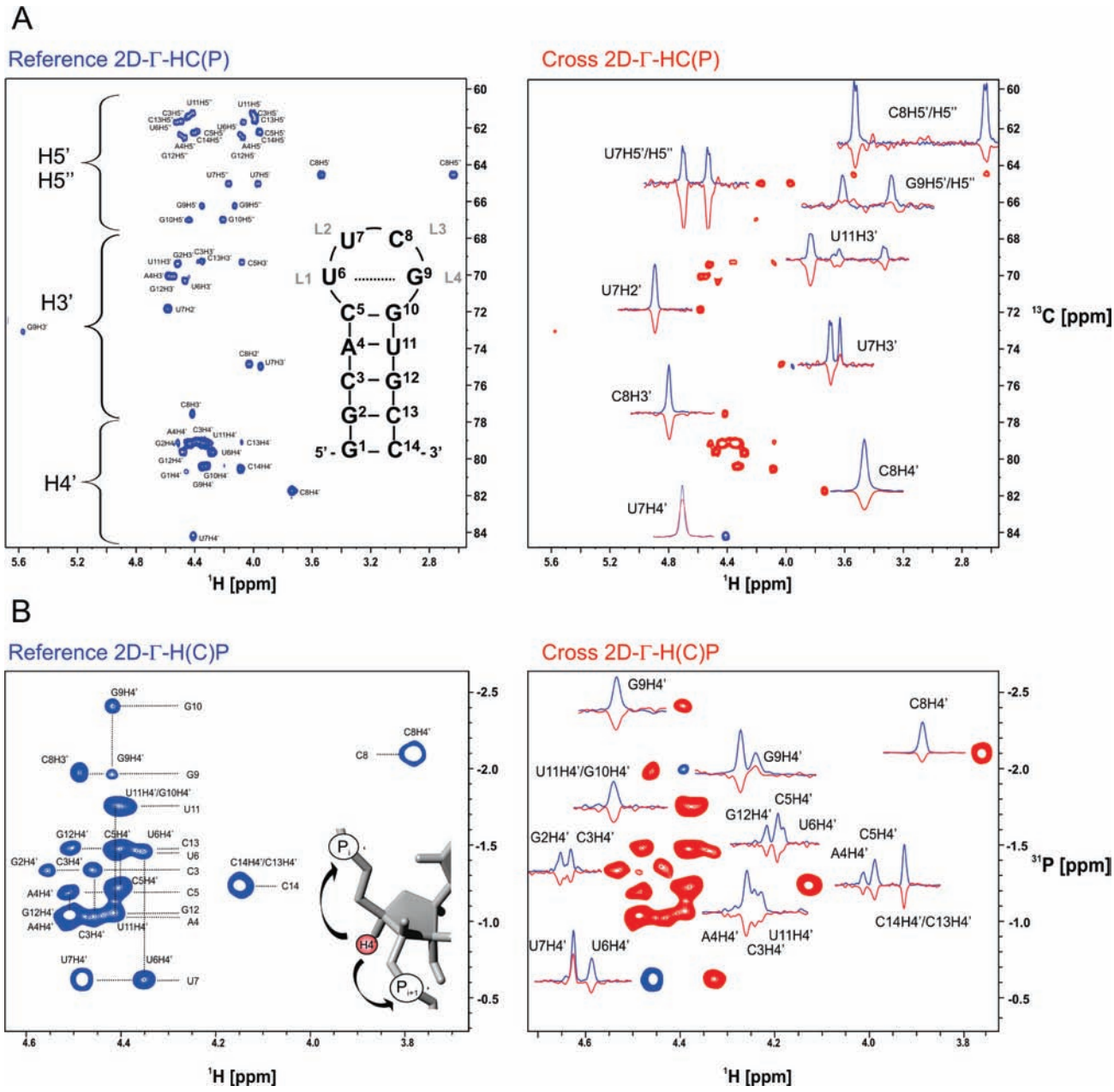

Figure 3. Quantitative reference and cross 2D Γ-HCP spectra of the 14-mer cUUCGg tetraloop RNA, recorded at 600 MHz and 298 K using an ^{1}H(^{13}C,^{31}P)-TCI cryogenic probe with *z* gradient. The on-resonance frequencies for ^{13}C and ^{31}P were set to 77 and −1.5 ppm, respectively. All of the proton pulses were applied at the water resonance. The field strengths for the ^{1}H and ^{13}C pulses were 23.8 and 16.7 kHz, respectively. During acquisition, GARP decoupling sequences were applied with field strengths of 2.5 and 0.8 kHz for ^{13}C and ^{31}P, respectively. (A) Quantitative ^{1}H,^{13}C 2D Γ-HC(P) experiment: (left) Reference experiment and schematic illustration of the secondary structure of the 14-mer cUUCGg tetraloop RNA. The tetraloop is additionally labeled L1−4, and the trans-wobble base pair U6−G9 is indicated by a dashed line. (right) Cross experiment, with 1D slices from the reference (blue) and cross (red) experiments shown for selected peaks. The reference experiment was recorded with 32 scans for 1 h with 80 and 2000 complex points in t_1 and t_2, respectively. The acquisition time was set to 170 ms, and t_1^{max} was 10 ms. A relaxation delay of 1.25 s was used. The cross experiment was recorded for 17 h with 512 scans. (B) Quantitative ^{1}H,^{31}P 2D Γ-H(C)P experiment selective for the C4′H4′ group. (left) Reference experiment. Horizontal lines connect signals arising from the same phosphate, and vertical lines indicate signals arising from the same proton to its own and the following phosphate, as depicted in the secondary structure of the shown nucleotide. The reference experiment was recorded with 256 scans for 4.5 h with 20 and 2000 complex points in t_1 and t_2. The acquisition time was set to 170 ms. A relaxation delay of 1.25 s was used. (right) Cross experiment. This experiment was recorded for 35 h with 2000 scans.

rate $\Gamma^{DD,CSA}_{(C3_iH3_i),P_{i+1}}$ depends on ε and ζ. The dipole of a C4′H4′ bond interacts with the CSAs of its own and the following phosphorus spin ($^{31}P_i$ and $^{31}P_{i+1}$, respectively). The obtained relaxation rates $\Gamma^{DD,CSA}_{(C4'_iH4'_i),P_i}$ and $\Gamma^{DD,CSA}_{(C4'_iH4'_i),P_{i+1}}$ are influenced by three torsion angles (α, β, γ and δ, ε, ζ, respectively). Following the mathematical derivation as previously introduced,[14] $\Gamma^{DD,CSA}_{CH,P}$ rates as a function of the involved backbone angles can be determined. The calculation of the conformational dependence of $\Gamma^{DD,CSA}_{CH,P}$ results in 2D and 3D correlations that can be represented by contour plots connecting pairs and triples of torsion angles, as shown in Figure 4. In view of the mathematical equation, it is obvious that the relation between the cross-correlated relaxation rate and the torsion angle is degenerate (Figure 4A).

Translation of Cross-Correlated Relaxation Rates into Torsion Angle Restraints. A translation of cross-correlated relaxation rates into torsion angles is up to fourfold-degenerate. We suggest the utilization of additional NMR data such as

Table 1. Cross-Correlated Relaxation Rates Determined for the 14-mer cUUCGg Tetraloop RNA

	$\Gamma^{DD,CSA}_{(C3'_iH3'_i),P_{i+1}}$ (Hz)[a]	$\Gamma^{DD,CSA}_{(C4'_iH4'_i),P_i}$ (Hz)[b]	$\Gamma^{DD,CSA}_{(C4'_iH4'_i),P_{i+1}}$ (Hz)[b]	$\Gamma^{DD,CSA}_{(C5'_iH5'_i pro\text{-}R),P_i}$ (Hz)[a]	$\Gamma^{DD,CSA}_{(C5'_iH5''_i pro\text{-}S),P_i}$ (Hz)[a]
experiment	$^1H,^{13}C$ 2D Γ-HC(P)	$^1H,^{31}P$ 2D Γ-H(C)P and $^1H,^{13}C,^{31}P$ 3D Γ-HCP	$^1H,^{31}P$ 2D Γ-H(C)P and $^1H,^{13}C,^{31}P$ 3D Γ-HCP	$^1H,^{13}C,^1H$ 3D Γ-HC(P)	$^1H,^{13}C,^1H$ 3D Γ-HC(P)
nucleotide					
G1[c]	–[c]	–[c]	–[c]	–[c]	–[c]
G2[c]	–[c]	–[c]	−17.7 ± 0.7	n.d.	n.d.
C3	−6.3 ± 1.1	−14.1 ± 1.8	−17.4 ± 0.7	−5.9 ± 1.1	4.7 ± 1.0
A4	−6.5 ± 1.2	−12.7 ± 3.4	−17.3 ± 1.0	n.d.	n.d.
C5	−4.8 ± 0.9	−14.3 ± 3[a]	−16.3 ± 1.0	−4.2 ± 0.8	2.7 ± 0.6
U6	−4.6 ± 0.8	−13.8 ± 1.0	−12.0 ± 0.7	−2.0 ± 0.4	3.4 ± 0.7
U7	1.2 ± 0.2	14.3 ± 0.8	n.d.	−10.4 ± 1.9	−7.7 ± 1.7
C8	−3.7 ± 0.7	−8.1 ± 0.5	n.d.	−8.3 ± 1.5	2.5 ± 0.6
G9	−4.3 ± 0.8	12.5 ± 1.6	−15.0 ± 1.1	4.6 ± 0.8	−0.4 ± 0.1
G10	n.d.	n.d.	−17.7 ± 3	−2.4 ± 0.4	−0.2 ± 0.0
U11	−6.2 ± 1.1	−17.3 ± 3[a]	−15.8 ± 2.6	−1.2 ± 0.2	6.5 ± 1.4
G12	−4.7 ± 0.9	−18.1 ± 3[a]	−16.2 ± 3	−3.2 ± 0.6	1.8 ± 0.4
C13	−3.7 ± 0.7	−18.3 ± 3[a]	n.d.	−5.4 ± 1.0	4.3 ± 1.0
C14[d]	–[d]	−15.7 ± 1.8	–[d]	−5.4 ± 1.0	4.2 ± 0.9

$\Gamma^{DD,CSA}_{(C2'_iH2_i),P_{i+1}}$ was also determined to be −3.2 ± 0.6 and −3.0 ± 0.6 Hz for residues U7 and C8, respectively.

[a] Calculation of errors was based on assuming an error of 10% in the signal intensities in the reference and cross experiments. [b] $\Gamma^{DD,CSA}_{(C4'_iH4'_i),P_i}$ and $\Gamma^{DD,CSA}_{(C4'_iH4'_i),P_{i+1}}$ were obtained from the $^1H,^{13}C,^{31}P$ 3D Γ-HCP and $^1H,^{31}P$ 2D Γ-H(C)P experiments and averaged. [c] The ^{31}P signals of nucleotides G1 and G2 were not detectable because of higher dynamics and conformational flexibility at the terminal end. [d] The last nucleotide, C14, ends with a 3′-OH group, with no 3′-PO_4^{2-} group attached.

nuclear Overhauser effects (NOEs) to confirm the appropriate torsion angles. Here, we calculated the structure with only NOE distance restraints in order to estimate the appropriate conformation. The recommended approach for deriving torsion angle restraints in an RNA structure calculation is schematically summarized in Figure 4.

Figure 4B shows the average spread in the torsion angle found in the structure bundle of the 14-mer cUUCGg tetraloop RNA calculated using only NOE distance restraints. The fact that the backbone torsion angles are insufficiently defined because of the low number of NOEs along the backbone is obvious. While the torsion angles α and γ showed a large spread of up to 40°, the distribution found for the torsion angle ζ remained small enough to reveal the tendency of the actual angle (Figure 4C). The difficulty of determining the angle α from NOE data alone, however, was alleviated because two cross-correlated relaxation rates for both the H5′ and H5″ protons could be determined. Thus, the number of possible solutions is reduced when cross-correlated relaxation rates from H5′ and H5″ protons can be resolved and incorporated. Further analysis was based on the assumption that the phosphodiester conformation is rigid.[38] The torsion angle α can be extracted from the three different cross-correlated relaxation rates $\Gamma^{DD,CSA}_{(C5'_iH5'_i pro\text{-}R),P_i}$, $\Gamma^{DD,CSA}_{(C5'_iH5''_i pro\text{-}S),P_i}$, and $\Gamma^{DD,CSA}_{(C4'_iH4'_i),P_{i+1}}$ using the torsion angle β determined from heteronuclear ^3J(C,P) and ^3J(H,P) coupling constants and the torsion angle γ obtained from ^3J(H,H) coupling constants. Cross-correlated relaxation rates of the C3′H3′ and the C4′H4′ groups to the succeeding phosphate (i.e., $\Gamma^{DD,CSA}_{(C3'_iH3'_i),P_{i+1}}$ and $\Gamma^{DD,CSA}_{(C4'_iH4'_i),P_i}$, respectively) yield information about the torsion angle ζ. Torsion angles ε and δ are known from heteronuclear ^3J(HP)/^3J(CP) coupling constants and from sugar conformations obtained from cross-correlated relaxation rates.[16,24] For the analysis of $\Gamma^{DD,CSA}_{(C4'_iH4'_i),P_i}$ and $\Gamma^{DD,CSA}_{(C4'_iH4'_i),P_{i+1}}$, we used the canonical conformations for the torsion angles γ and δ. We observed that some $\Gamma^{DD,CSA}_{(C4'_iH4'_i),P_i}$ values exceeded the maximal value by 1−3 Hz. In these cases, data were fit to the next maximum, which was close to the expected conformation. The resulting data agree well with other cross-correlated relaxation rates (Figure S3 in the Supporting Information).

Table 2 summarizes the torsion angles for the 14-mer cUUCGg tetraloop RNA derived from interpretation of scalar coupling constants measured previously and the relaxation rates. In general, the resulting torsion angles for α and ζ obtained from different cross-correlated relaxation rates are very consistent, indicating the good quality of the data. Structure calculations using the obtained data demonstrated that the additional restraints for α and ζ improved the precision of the structure to a degree comparable to the incorporation of 32 RDCs of the NH, C1′H1′, C6H6, and C8H8 groups (Figure 4D). For the determination of the angle α, the NMR data are in line with the torsion angles derived from the X-ray structures (Figure 5). It is rather striking that the α torsion angles derived from the Γ rates fit the averaged X-ray values remarkably well, although the α torsion angles show a large spread of values in different X-ray structures. This fact might support the idea that the loop structure in solution relaxes to a single main conformation while crystals can capture one out of several different possible low-energy conformations. In contrast to α, the torsion angle ζ was found to be less variable within the X-ray structures, except for the residue U7, where larger variations were observed for this angle. The results for the torsion angle ζ agree well with the cUUCGg X-ray structures, except for the residue U7. At this site, the cross-correlated data do not represent the average X-ray conformation but rather fit one single X-ray structure (PDB entry 1f7y).[39] For the stem region, the torsion angles α and β are consistent with the canonical A-form conformation. The structure calculation using all of the torsion angles yielded a high-resolution structure with an RMSD of 0.37 Å[38] (Figure 4D), which indicates that the determined torsion angles α and ζ are consistent with other NMR data such as NOE distances and other dihedral angle restraints. The extracted torsion angles confirmed the unusual ^{31}P chemical shift of residues U7, C8, and G9, which adopt noncanonical conformations, but the ^{31}P chemical shift of residue G10 cannot be explained by the present conformation.

Discussion and Conclusion

This work presents the development of 2D and 3D Γ-HCP experiments optimized for the CH and CH_2 groups that enables the measurement of five CH-dipolar,^{31}P-CSA cross-correlated relaxation rates and the subsequent determination of the backbone torsion angles α and ζ in RNA/DNA oligonucleotides. The method is based on the measurement of cross-correlated relaxation rates in a quantitative manner and has been applied

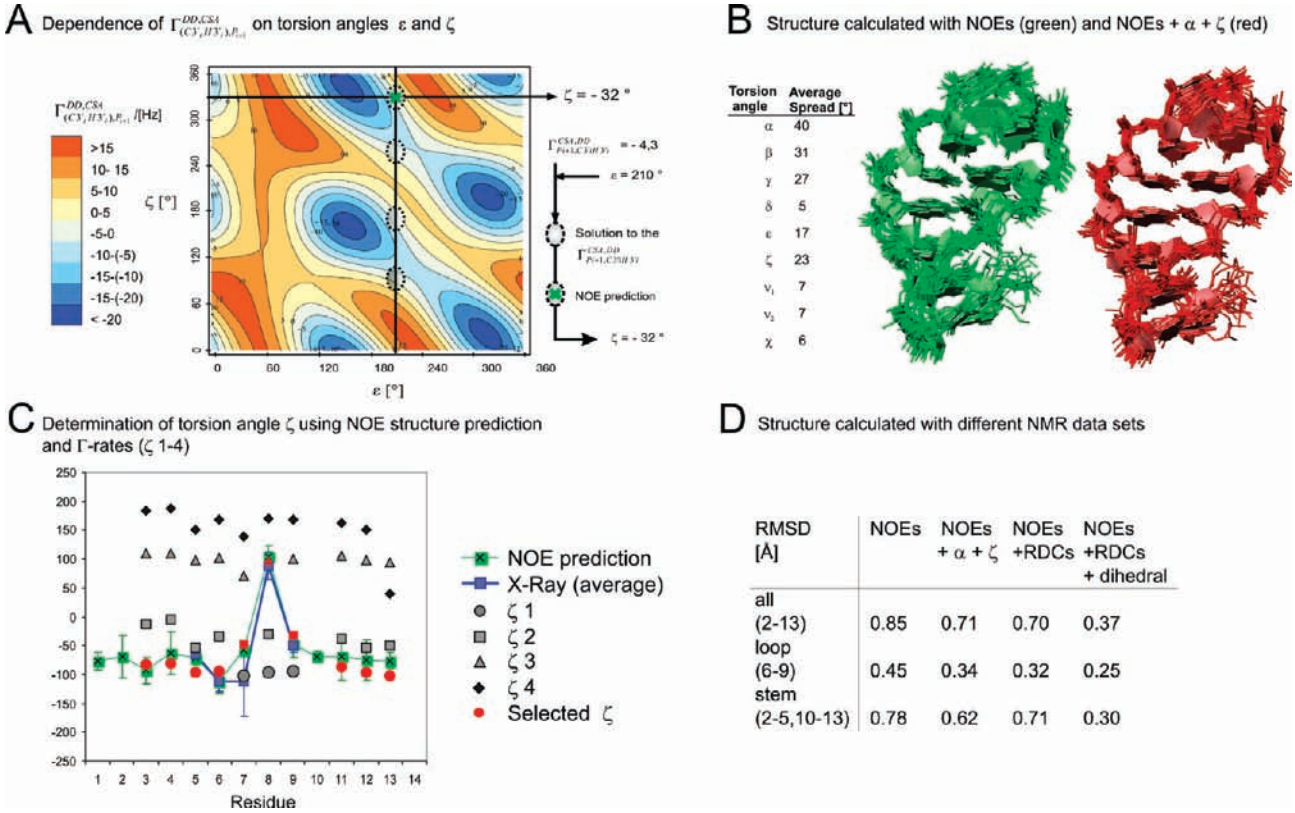

RMSD [Å]	NOEs	NOEs + α + ζ	NOEs +RDCs	NOEs +RDCs + dihedral
all (2-13)	0.85	0.71	0.70	0.37
loop (6-9)	0.45	0.34	0.32	0.25
stem (2-5,10-13)	0.78	0.62	0.71	0.30

Figure 4. (A) Dependence of $\Gamma^{DD,CSA}_{(C3'_i H3'_i),P_{i+1}}$ on the phosphodiester backbone torsion angles ε (horizontal axis) and ζ (vertical axis). Values for nucleotide G9 are shown. From the coupling constants, an ε value of 210° can be determined. The value $\Gamma^{DD,CSA}_{(C3'_i H3'_i),P_{i+1}} = -4.3$ Hz allows for four possible combinations of ε and ζ angles. The NOE prediction allows the appropriate torsion angle ζ to be estimated as −32°. (B) Bundle of 20 structures with the lowest energy calculated using only NOE distance restraints (green) and NOEs including restraints for α and ζ (red). The average spread in the torsion angle within the NOE structure bundle is shown at the left. (C) Determination of the torsion angle ζ from $\Gamma^{DD,CSA}_{(C3'_i H3'_i),P_{i+1}}$, which leads to four possible solutions ($\zeta 1-\zeta 4$). The NOE-based prediction for ζ according to the structure calculation is highlighted in green, and the final solution is depicted in red. (D) Root-mean-square deviation (RMSD) values for structure bundles calculated using different NMR restraint data sets.

Table 2. Comparison of the Torsion Angles α, β, ε, and ζ Determined Here Using NMR Analysis with Those from X-ray Structures

	values from NMR analysis (deg)				values from X-ray structures (deg)[a]			
NMR parameter	α^b $\Gamma^{DD,CSA}_{(C5'_i H5'pro\text{-}R),P_i}$ $\Gamma^{DD,CSA}_{(C5'_i H5''pro\text{-}S),P_i}$ $\Gamma^{DD,CSA}_{(C4'_i H4'_i),P_i}$	β ^3J(C,P) ^3J(H,P)	ε ^3J(C,P) ^3J(H,P)	ζ^b $\Gamma^{DD,CSA}_{(C3'_i H3'_i),P_{i+1}}$ $\Gamma^{DD,CSA}_{(C4'_i H4'_i),P_{i+1}}$	α	β	ε	ζ
nucleotide								
G1	$-^d$	180 ± 40	228 ± 20	$-^d$				
G2	$-^d$	180 ± 40	n.d.	$-^f$				
C3	−83 ± 5 (35)	177 ± 30	194 ± 40	−80 ± 3 (50)				
A4	n.d.	n.d.	189 ± 20	−79 ± 1 (30)				
C5	−86 ± 8 (25)	176 ± 15	220 ± 15	−66 ± 11 (30)		173 ± 4	211 ± 2	−65 ± 3
U6	−85 ± 6 (35)	176 ± 25	207 ± 15	−100 ± 7 (30)	−66 ± 4	180 ± 4	204 ± 10	−111 ± 18
U7	176 ± 7 (60)	180 ± 60	300 ± 60	-48^c (30)	161 ± 65	179 ± 32	324 ± 80	−112 ± 60
C8	−74 ± 15 (35)	184 ± 20	215 ± 60	99^c (60)	−66 ± 21	167 ± 36	267 ± 30	89 ± 23
G9	76 ± 7 (50)[e]	$-^e$	212 ± 15	−46 ± 14 (30)	64 ± 18	187 ± 25	220 ± 17	−49 ± 12
G10	−94 ± 9 (50)[e]	$-^e$	194 ± 40	-75^c (40)	−101 ± 75	164 ± 50		
U11	−85 ± 3 (40)	184 ± 30	212 ± 20	−83 ± 4 (30)				
G12	-81^c (40)	n.d.	217 ± 20	−97 ± 0 (30)				
C13	−84 ± 5 (35)	180 ± 20	217 ± 20	-102^c (50)				
C14	−84 ± 5 (60)	175 ± 40	$-^g$	$-^g$				

[a] X-ray structures of the cUUCGg tetraloop in 14-mer RNA, nucleotides 5−10 (PDB entries 1f7y, 1fjg, and 1i6u). [b] Torsion angles obtained by averaging over all results derived from interpretation of scalar coupling constants measured previously and the relaxation rates. The given errors were derived from the deviation between angles obtained from different Γ rates, if present. In parentheses are given the errors obtained by taking into account the errors in the torsion angles β and ε. These values were used in the structure calculations. [c] Torsion angle was derived from a single Γ rate. [d] ^{31}P signals of the nucleotides G1 and G2 were not detectable because of higher dynamics and conformational flexibility at the terminal end. [e] Coupling constants could not be fit to either single or multiple conformations. β was taken from the final structure (G9, 200°; G10, 180°) calculated without incorporation of α and ζ restraints. [f] Torsion angle could not be determined because of the missing torsion angle ε for nucleotide G2. [g] The last nucleotide, C14, ends with the 3′-OH group, with no 3′-PO_4^{2-} group attached.

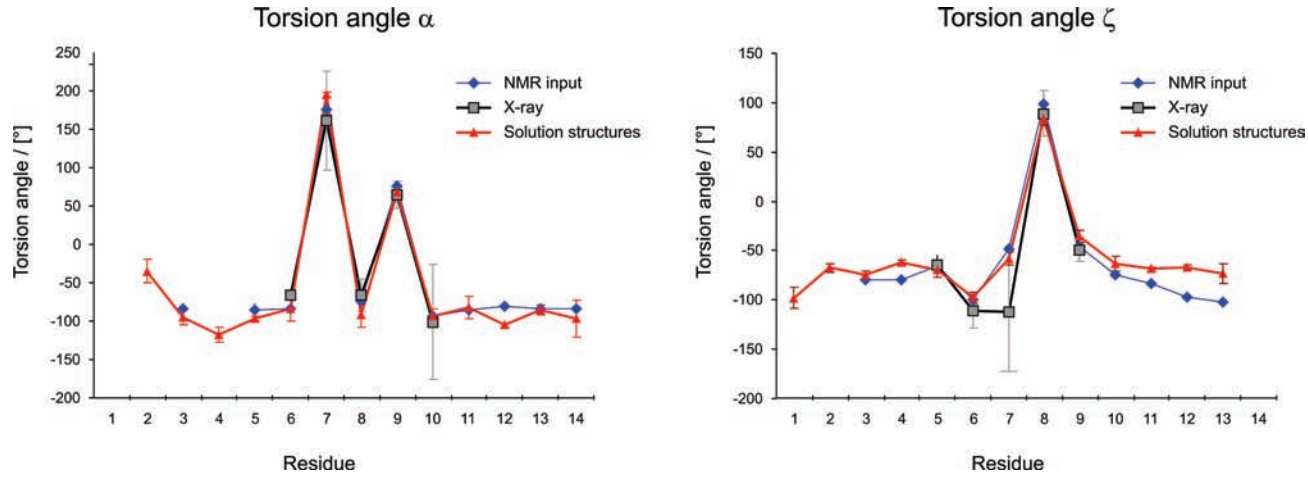

Figure 5. Comparison of torsion angles α and ζ from (blue) NMR data (Γ rates, *J* coupling constants), (gray) average values of the X-ray structures (PDB entries 1f7y, 1fjg, and 1i6u), and (red) the new NMR solution structure (PDB entry 2koc). Error bars indicate the conformational spreads within the respective structure bundles.

to the ^{13}C-labeled 14-mer cUUCGg tetraloop RNA model system. In the original experiment, ^{13}C,^{31}P DQC/ZQC was allowed to evolve under scalar *J*(C,H) coupling and cross-correlated relaxation $\Gamma^{DD,CSA}_{CH,P}$ during a constant-time evolution period. This resulted in a doublet with different intensities due to the differential relaxation of the H^{α} and H^{β} components of the multiplet, as outlined by Richter et al.[14] In the new experiments, decoupling takes place, leading intrinsically to higher resolution and a higher single-to-noise ratio. Furthermore, the design of the new pulse sequences allows for differentiation of $\Gamma^{DD,CSA}_{(C5'_iH5''_i\text{pro-}R),P_i}$ and $\Gamma^{DD,CSA}_{(C5'_iH5''_i\text{pro-}S),P_i}$ as well as $\Gamma^{DD,CSA}_{(C4'_iH4'_i),P_i}$ and $\Gamma^{DD,CSA}_{(C4'_iH4'_i),P_{i+1}}$. Carlomagno et al.[44] have discussed the advantages of *J*-resolved and quantitative Γ experiments for the determination of such cross-correlated relaxation rates. In the case of larger RNAs, the advantage in resolution obtained in the quantitative experiment is the important improvement relative to the previous method. This in turn allows us to determine a lower limit for the size of the cross-correlated relaxation rate that is determined by the signal-to-noise ratio in our experiments. Fluctuations of signal intensities by ±10% give rise to changes in rates by approximately the same amount because of the nearly linear relationship between signal intensity and rate. The variation of the resulting torsion angle is mostly on the order of a few degrees, since the correlation depends on the rate in a very sensitive manner.

The applicability of our new method was further demonstrated on the 27-mer neomycin riboswitch RNA (Figure 6). We obtained well-resolved spectra (Figure 6A,B) that yielded 23 $\Gamma^{DD,CSA}_{(C3'_iH3'_i),P_{i+1}}$ and 17 $\Gamma^{DD,CSA}_{(C4'_iH4'_i),P_{i+1}}$ values that could be translated to torsion angles ε and ζ for 16 out of 26 residues without the use of any additional *J* coupling constants. Two additional torsion angles ζ could be determined when information from ^3J(C4′,P_{i+1}) coupling constants was taken into account. Figure 6C shows that the Γ rates reflect a similar conformation for ε and ζ, as seen in the structure bundle calculated using only NOE distance restraints and limited scalar coupling information without ε/ζ input restraints.[20] Major differences are apparent in the torsion angle ζ of residues U8, U14, and A17 within the bulge.

For the determination of angles from cross-correlated relaxation rates, the effect of local dynamics must be taken into account. Order parameters scale the cross-correlated relaxation rate. For high cross-correlated relaxation rates, a lower order parameter might influence the resulting torsion angle. In contrast, if the cross-correlated relaxation rates are low, the order parameter does not effect the torsion angle determination. In our previous work, autocorrelated order parameters for the carbon nuclei in the ribose moiety and the phosphate nuclei of the backbone were determined.[27,38] Under the assumption of fast, uncorrelated movement of the CH bond vectors and the phosphate group, the cross-correlated order parameter can be calculated using the expression $(^{cross}S^{DD,CSA}_{P,C3'H3'})^2 = (^{auto}S^{CSA,CSA}_{P,P})(^{auto}S^{DD,DD}_{C3'H3',C3'H3'})$. Overall, the cross-correlated order parameters showed only a small variation within the 14-mer RNA and had a mean value of 0.86 ± 0.04. The lowest cross-correlated order parameter was found for U7 and had a value of 0.79, which is only slightly lower than the average order parameter. In addition, the measured Γ rates for U7 are small, so the effect of the order parameter on the torsion angle determination is small.

In regard to the magnetization pathway, the cross and reference experiments differ in the additional proton recoupling delay (Δ″; Figure 2A), which can lead to loss of intensity as a result of relaxation effects. However, from the analysis of $\Gamma^{DD,CSA}_{(C6/8,H6/8),N1/N9}$ and $\Gamma^{DD,CSA}_{(C1',H1'),C2'}$, it is known that the effect is less than 1%[17,45] and therefore can be neglected. The precision of the extracted torsion angles is further affected by the possible error in the determination of the second or third torsion angle involved in the projection. These uncertainties might be due either to inappropriate Karplus parametrizations for ^3J(C,P) and ^3J(H,P) coupling constants or to RNA flexibility.

The interpretation of the data further relies on detailed knowledge of the magnitude and orientation of the ^{31}P CSA tensor, which is another important factor that must be considered. In a recent DFT study, Přecechtělová et al.[26] extensively investigated the ^{31}P CSA tensor for different conformations of RNA. They found that for different conformations, the components of the traceless CSA tensor vary by 16−22 ppm. Moreover, the CSA tensor adopts a slightly different orientation with respect to the molecular coordinate system, which might have a significant effect on the obtained torsion angles. The influence of these two variations (magnitude and orientation)

(44) Carlomagno, T.; Griesinger, C. *J. Magn. Reson.* **2000**, *144*, 280.

(45) Fiala, R.; Czernek, J.; Sklenar, V. *J. Biomol. NMR* **2000**, *16*, 291.

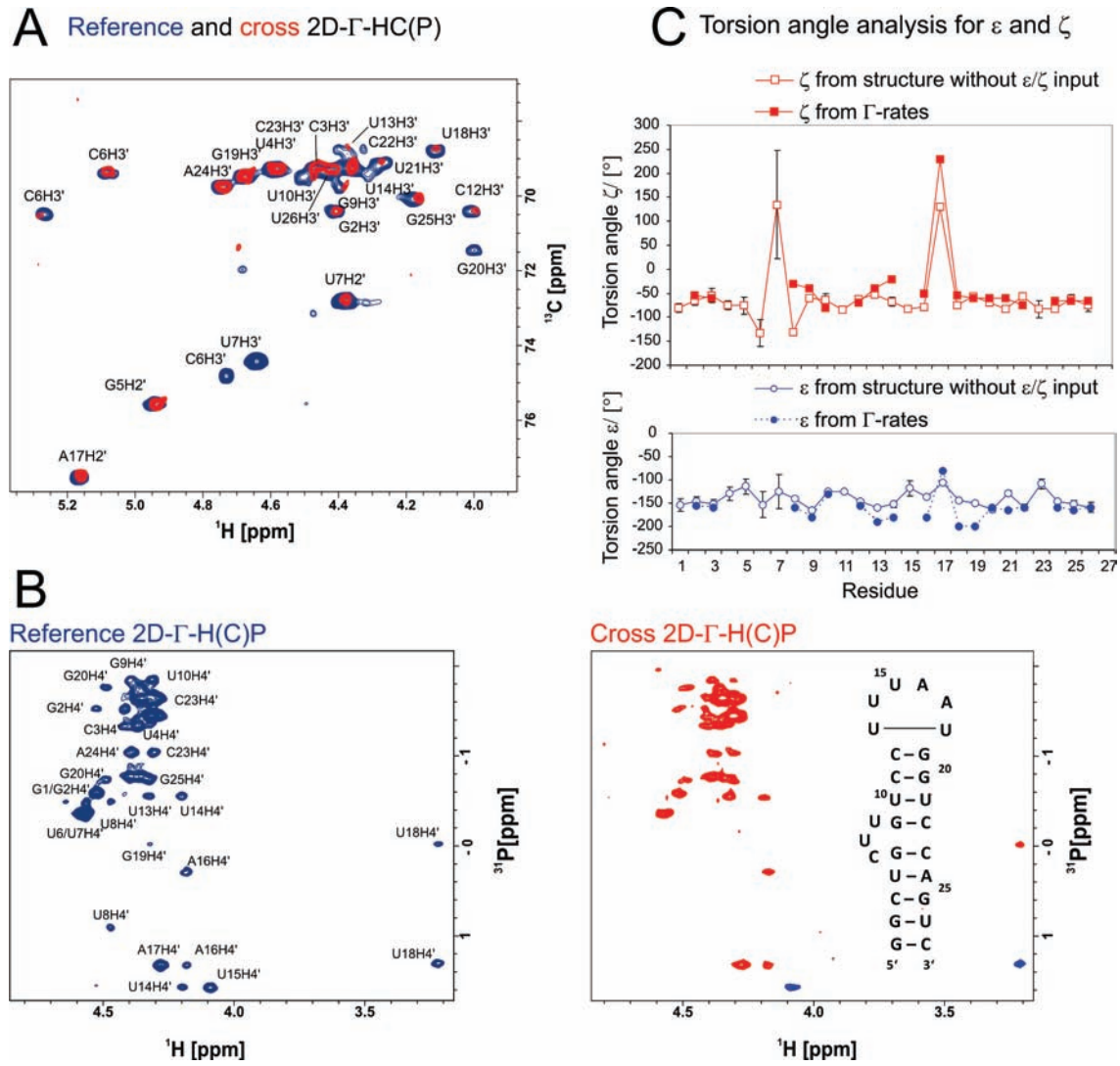

Figure 6. Quantitative Γ-HCP spectra of the 27-mer neomycin riboswitch RNA[20] recorded at 600 MHz and 298 K using an $^{1}H(^{13}C,^{31}P)$-TCI cryogenic probe with *z* gradient. (A) Expansion of the quantitative $^{1}H,^{13}C$ 2D Γ-HC(P) reference (blue) and cross (red) spectra for the C3′H3′ group region. (B) Quantitative $^{1}H,^{31}P$ 2D Γ-H(C)P reference (blue) and cross (red) experiments selective for the C4′H4′ group. The inset of the cross spectrum shows a schematic illustration of the secondary structure of the 27-mer neomycin riboswitch. (C) Torsion angle analysis for ε and ζ from $\Gamma^{DD,CSA}_{(C3'_iH3'_i),P_{i+1}}$ and $\Gamma^{DD,CSA}_{(C4'_iH4'_i),P_{i+1}}$ and comparison with the torsion angles extracted from the structure bundle calculated without ε and ζ input restraints.[20]

of the ^{31}P CSA tensor were analyzed here. The results showed that the changes have an effect on the Γ rates in some RNA conformations but generally remain small enough (Figure S4 in the Supporting Information) that it seems sufficient to employ the same ^{31}P CSA tensor to all of the phosphate groups. In general, both methods, cross-correlated relaxation rates and ^{31}P-rCSA, depend on the accuracy of the ^{31}P CSA tensor used.

In this work, we have presented a method for measuring five different cross-correlated relaxation rates that depend on six torsion angles along the phosphodiester backbone. We used additional NMR data (scalar coupling constants) to translate the Γ rates into further torsion angles. Notably, it was possible to show that although the Γ data are degenerate (Figure 4), careful analysis of the allowed conformational α, β (or ε, ζ) torsion angle space in conjunction with analysis of NOE data alone alleviates this degeneracy in most cases. In fact, if we assume that the sugar conformation is known from other experiments, the favorable situation where five experimental parameters describe five degrees of freedom arises. In this case, there is no need to measure coupling constants, and it would be sufficient to include only cross-correlated relaxation rates into the structure calculation in order to describe the complete backbone conformation. We have presented this approach for the 27-mer RNA, for which $\Gamma^{DD,CSA}_{(C3_iH3_i),P_{i+1}}$ and $\Gamma^{DD,CSA}_{(C4'_iH4'_i),P_{i+1}}$ were exploited to determine the two torsion angles ε and ζ using only the NOE-based NMR structure without additional experimental restraints (e.g., from *J* coupling constant data).

It is of further interest to look at the information content gained by the qualitative interpretation of cross-correlated relaxation rates, which can already provide a useful picture of the RNA/DNA conformation in addition to the torsion angles α and ζ. Schneider et al.[10] analyzed the structure of the rRNA and identified 18 non-A-type and 14 A-RNA-related conformational classes described by two nucleotides. We used those 32 RNA conformational classes to calculate the cross-correlated relaxation rates expected for the first nucleotide of the respective conformation (Figures 7 and 8). In addition to the single cross-correlated relaxation rates, we calculated the resulting sum of the rates for the C5′H5′/H5″ and C4′H4′ groups (Figure 7f,g) as they appeared in the $^{1}H,^{13}C$ 2D HC(P) experiment (Figure 3A). Each RNA class leads to a unique pattern for the size and sign of the cross-correlated relaxation rates that immediately

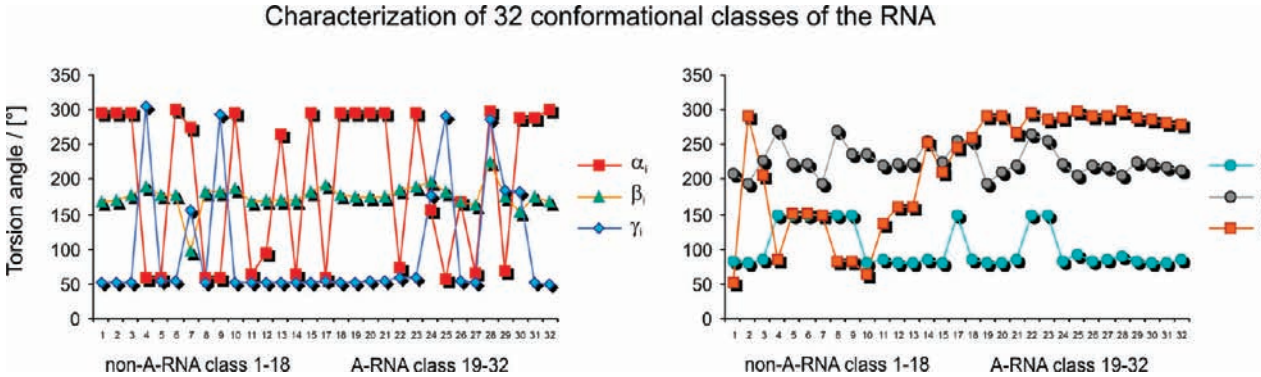

Figure 7. Characterization of the conformation of the first nucleotide in RNA conformational classes 1−32 according to Schneider et al.[10]

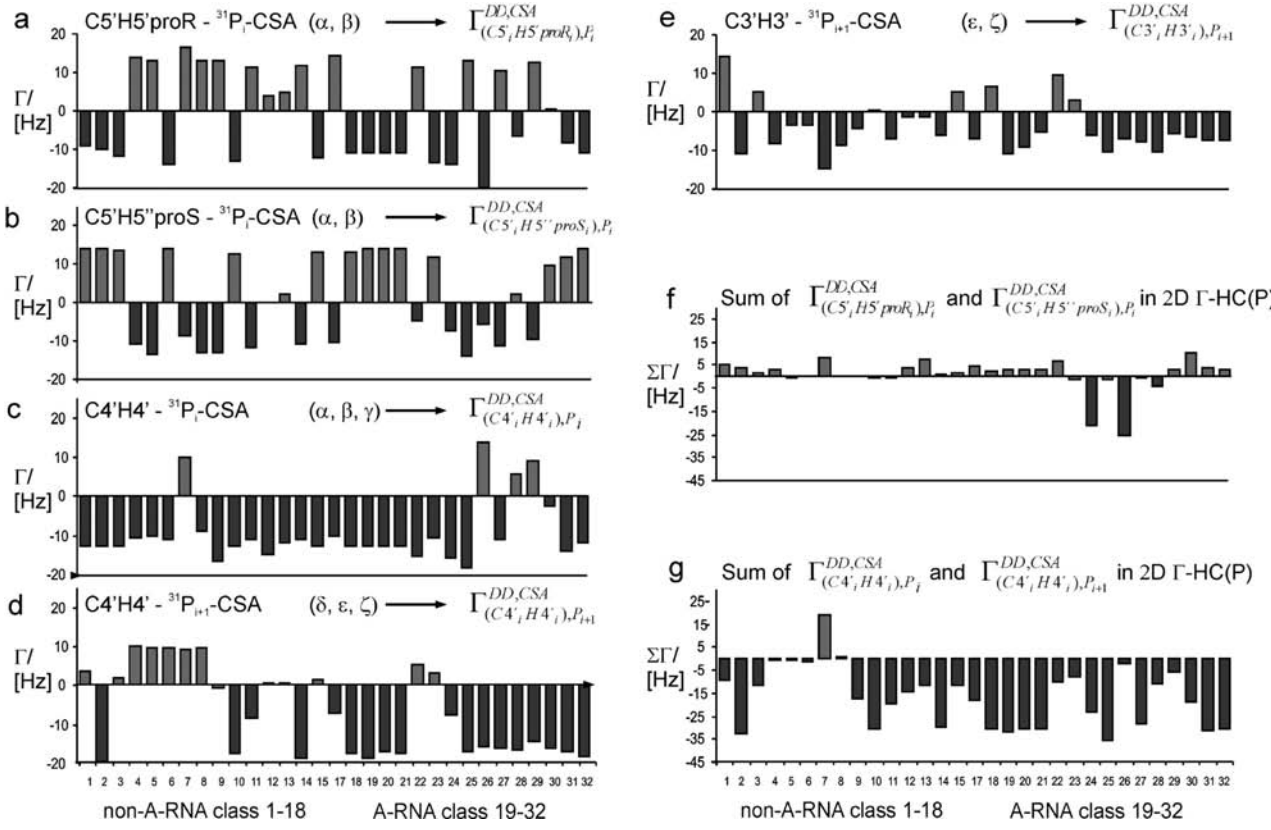

Figure 8. Theoretical values for (a) $\Gamma^{DD,CSA}_{(C3'_iH3'_i),P_{i+1}}$, (b) $\Gamma^{DD,CSA}_{(C4'_iH4'_i),P_i}$, (c) $\Gamma^{DD,CSA}_{(C4'_iH4'_i),P_{i+1}}$, (d) $\Gamma^{DD,CSA}_{(C5'_iH5'_i\text{pro-}R),P_i}$, and (e) $\Gamma^{DD,CSA}_{(C5'_iH5''_i\text{pro-}S),P_i}$ calculated for the first nucleotide of 32 RNA conformational classes defined by the backbone torsion angles α, *β*, *γ*, *δ*, *ε*, and *ζ*, as shown in the Figure 7.[10] More detailed information about the torsion angles and exact Γ rate values can be found in Table S4 in the Supporting Information. Panels (f) and (g) show the sum of $\Gamma^{DD,CSA}_{(C5'_iH5'_i\text{pro-}R),P_i}$ and $\Gamma^{DD,CSA}_{(C5'_iH5''_i\text{pro-}S),P_i}$, $\Gamma^{DD,CSA}_{(C4'_iH4'_i),P_i}$, and $\Gamma^{DD,CSA}_{(C4'_iH4'_i),P_{i+1}}$ obtained from the ^{1}H,^{13}C 2D HC(P) experiment, where respective single cross-correlated relaxation rates cannot resolved because of the missing chemical shift evolution.

allows for a qualitative estimation of the conformational class without further calculations. For instance, looking only at the general signs of the rates measured for the stem of the 14-mer RNA (Table 1) allowed the number of possible RNA classes to be reduced to six A-type classes that deviated by 10° from the A-form RNA. The Γ rates obtained within the loop did not follow a clear trend, indicating the noncanonical conformation of the loop residues. In particular, the strong signals of the C5′H5′ group of the residue U7 seen in the ^{1}H,^{13}C 2D HC(P) cross experiment (Figure 3A) are indicative of a noncanonical conformation, as those are not expected to appear very strong for most of the conformational classes according to their resulting sum (Figure 7f). In the ^{1}H,^{31}P 2D H(C)P spectra (Figure 3B), singles of the residue U7 and G9 strikingly show positive signals and thus positive Γ rates, which is not expected for an A-RNA conformation.

The utility of the method has been demonstrated by the structure determination of the 14-mer cUUCGg tetraloop RNA using the resulting torsion angles α and *ζ* for the structure calculation. In combination with other NMR data (NOEs, dihedral angles, and RDCs), structure calculations yielded a very precise structure[24] in which the torsion angles α and *ζ* showed high convergence and were remarkably consistent with the experimental results. It was possible to achieve cross-validation of the cUUCGg tetraloop, for which both X-ray and NMR structures have been determined. The comparison of the torsion angles derived from the analysis of cross-correlated relaxation rates with previously known

structural data revealed an excellent overall agreement (Figure 5). Furthermore, it has been shown that the new method is suitable for larger RNA, as demonstrated by experiments on the 27-mer neomycin riboswitch RNA.

Acknowledgment. We dedicate this work to Prof. Christian Griesinger on the occasion of his 50th birthday. The work was supported by the State of Hesse (BMRZ), the DFG (SFB579: "RNA−Ligand Interaction"), and the Studienstiftung des Deutschen Volkes through Grants to S.N. and B.F. H.S. is member of the DFG-funded Cluster of Excellence: Macromolecular Complexes. The authors acknowledge insightful discussions with Hendrik R. A. Jonker on determination of the structure of RNA and Prof. Jens Wöhnert and Prof. Beatrix Süss on the neomycin aptamer.

Supporting Information Available: Two figures showing 2D and 3D contour plots for the torsion-angle dependence of all Γ rates; one diagram showing explicit results for the torsion angles α and ζ calculated from all available Γ rates and the torsion angles predicted from the structure calculated with only NOE distance restraints; two tables describing the torsion angles of 32 RNA conformational classes; one table with the direction and principal components of the ^{31}P CSA tensor with respect to the molecular frame in different RNA classes, as obtained by Přecechtělová et al.;[26] one diagram showing Γ rates calculated with theoretically and experimentally obtained ^{31}P CSA for different RNA classes; and one table with theoretical Γ rates calculated for the protons of the first nucleotide adopting 32 different conformational classes. This material is available free of charge via the Internet at http://pubs.acs.org.

JA910015N